Chapter

Energy and Exergy Analysis of an Advanced Cookstove-Based Annular Thermoelectric Cogeneration System

Sakthivadivel Duraisamy, Manikandan Sundararaj, Kumaraselvan Raja, Ganesh Kumar Poongavanam and Iniyan Selvarasan

Abstract

This chapter deals with the energy and exergy analysis of the cookstove-based gasifier annular thermoelectric generator (GATEG). The vented waste heat is made available at the outer surface of the combustion chamber of an advanced micro-gasifier cookstove for added energy feed to the GATEG. This combined device has a competence to satisfy both cooking needs and micro-electrification of rural villages by a simultaneous recovery of heat energy and power (CHP) as cogeneration system. The power output (W), electrical energy efficiency (%) and exergy efficiency (%) of the proposed advanced micro-gasifier cookstove-based ATEG are 10 W, 6.78 and 15%, respectively. The maximum hot side wasted temperature without annulus gain is 275°C, which translates equivalent loss values as 7.64 W, 5.45 and 10.49%; this loss is higher than achievable minimum hot side temperature of 150°C on which this analytical chapter is drafted. This detailed study will be extremely useful to the designers of commercial biomass advanced micro-gasifier cookstove integrated ATEG systems.

Keywords: cookstove, energy, exergy, power, annular thermoelectric generator

1. Introduction

Clean sources of enhanced energy recovery offer the best mitigating solution to the economic, environmental and climate effects from the continued high consumption/utilisation of fossil fuels. Biomass resource is an excessive source of carbon-neutral renewable energy (RE) available far and worldwide and is a good source of environment-friendly, clean energy resource. In the near future, the biomass energy is likely to be one of the most dominant REs, contributing to a substantial reduction in consumption of carbon-emitting fossil fuels and electricity for cooking as well as lighting. Many methods have been adopted to produce combined heat energy and power (CHP), in improved cookstoves with advanced features of the flat thermoelectric generator (FTEG). Easy availability, accessibility, low-cost per capita produced energy, reduced emissions and inbuilt driving force have led to greater attention to CHP cookstove systems. Subsequently, exploring an

efficient biomass advanced cookstove technology is necessary. An accurate inbuilt electricity generation unit to drive forced draft combustion fan/blower, to optimise performance with high efficiencies, is proposed in this current study.

For the previous two decades, the use of thermoelectric generators and its applications have been investigated and improved worldwide due to its significant advantages of straight conversion of thermal energy into electricity with minimum/no moving parts and reduced noise. Hence, newly developed thermoelectric generators (TEGs) are accepted as green sustainable technology and are widely used as flexible generators for a diversified applications [1, 2]. A combined advanced micro-gasifier cookstove with the TEG for heat and power cogeneration from a single system is presented here.

Champier et al. [3] have developed a prototype of a biomass cookstove with a higher-efficient combustion chamber (CC), and TEG modules are attached to either side of the cookstove. It was found from the experimental investigations that 6 W of electrical power was generated from four numbers of TEG. Experimental analysis was performed by Nuwayhid et al. [4] on the biomass domestic wood stove coupled with natural convection-cooled thermoelectric generator. It was obtained from the results that about 4.2 W of power was produced from each component. Kraemer et al. [5] built an innovative solar flat thermal panel for electricity generation adopting Seebeck effect concept with higher thermal concentration. There was an interesting result obtained from the study that an electrical convention efficiency of 4.6% for 1000 W/m^2 solar conditions is about eight times much more powerful than the other systems. Omer and Infield [6] proposed a conceptual model of a TEG for the estimation of an optimal device in power production. By means of using their developed model, four different TEGs were compared. Besides, they have developed a two-stage solar concentrator for a cogeneration system (combined heat and power from the thermoelectric modules). It was proven from the studies conducted by Omer and Infield [7] that an improvement of thermal efficiency as well as overall characteristics of the solar thermal concentrator for combined heat and thermoelectric power generation can be achieved using second stage concentrator.

Atik [8] studies the thermoelectric performances of the concentrating collector, receiver and TEG modules. The electric power generation efficiency, system efficiency and surface area temperature of the receiver system were obtained from the different solar radiation (W/m^2) and from different concentration ratios. Chen [9] suggested a model to examine the conceptual efficiency of solar thermoelectric generators (STEGs), which includes thermal concentration as well as optical concentration. It was obtained from his study that the component efficiency increases with increase in hot side temperature, but thermal efficiency decreases with increasing hot side temperature. Furthermore, he stated that the STEG efficiency can be improved when it has been maintained under evacuated condition.

Manikandan and Kaushik [1] performed the energy and exergy study of the solar annular thermoelectric generator (SATEG) in view of the impact of Thomson effect in concurrence with Peltier effect, Joule effect and Fourier heat conduction. Their study proposed annular thermoelectric generator as an alternative for flat thermoelectric generator (FTEG) to increase the cross-sectional area along the radial direction. They have established that the power output (W) and whole exergy efficiency (%) of the SATEG were 1.92 W and 5.02%, respectively, which was established to be 0.52 and 0.40% greater than that of SFTEG. They suggested that this SATEG system could be effectively used as the thermal insulation material as it offered better heat transfer characteristics; it was simple to drive and maintain compared to the solar flat plate thermoelectric generator.

From an in-depth literature survey, it is established that there are certainly no research studies available on CHP system in cookstove and an ATEG. Studies have

explored only the performance evaluation of energy efficiency and exergy efficiency of the cookstove with an FTEG. The advantage of using an ATEG instead of FTEG is that it enhances the heat transfer surface area on both hot side and cold side, due to cylindrical structure. It is proposed to study the behaviour of ATEG placed outside the cylindrical CC to convert waste heat (hot side) into electricity as well as dissipate heat (cold side) by passing and preheating air through annular fins. Hence, it is indeed essential to study the energy and exergy analysis of an advanced cookstove-based ATEG for clean combustion and self-sustained cooking options, particularly suited for developing countries. Here, the exergy analysis (second law of thermodynamics) is an advanced method to enumerate the real irreversibilities delivered in the thermodynamic process.

2. Materials and methods

2.1 System description

The design and fabricated CC of the proposed biomass advanced micro-gasifier cookstove [10–15] are clearly depicted in **Figure 1**. The CC is fabricated using carbon steel with an inner diameter of 110 mm and an inner height of 155 mm. By means of increase in the proportion percentage (%) of carbon content, the cylinder material becomes harder and stronger providing higher creep properties. Carbon steel with high carbon content has been used to ensure it can withstand high temperatures.

The secondary air (combustion air) injection of the proposed cookstove is skewed to an angle of 45° towards bottom grate [11, 12, 16]. This is to confirm the better turbulence in the course of volatile combustion and for the period of char combustion. Exfoliated vermiculite mineral matter of 93% with glass wool of 2%

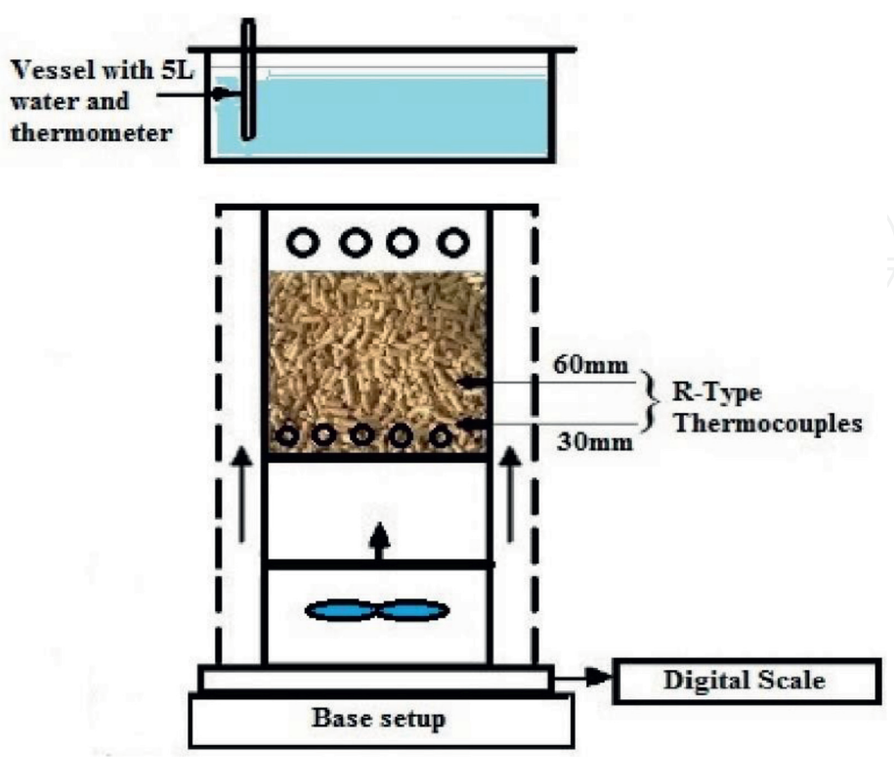

Figure 1.
Model of the proposed cookstove.

and Portland cement of 5% altogether by weight is moulded into a mixture for the preparation of the thermal protection lining material inside the concentric cylindrical CC. The air gap between two concentric cylindrical rings of the CC is filled with the same refractory composite paste. The thermal conductivity (k) of the prepared composite blend slab is calculated to be about 0.047 W/m°C by performing steady-state thermal conductivity test, as suggested by BIS-IS 9489 [17]. Due care is taken to ensure the total absence of any bypass channels due to the faulty lining of the thermal composite insulation material in the gasification and combustion air paths. A blower of the capacity 12 V DC is fitted below the combustion chamber of the cookstove. It tends to force the ambient air upwards along the way through the side of the CC; gasification and combustion ducts of diameter 4 and 3 mm provide the needed gasification and combustion air.

In the advanced micro-gasifier cookstove-based ATEG system, the exterior surface of the CC is in connection with the hot side junction of the GATEG. Hence, the waste heat ejected or lost is effectively used by the ATEG for the generation of electric power. The remaining heat energy available at the cold side junction of ATEG is exploited for preheating the secondary combustion air. The primary heat generated by the advanced micro-gasifier system is used for cooking food on the stove. This combined cogeneration cookstove system can deliver both electric power to drive fan/blower (also lighting, micro-charger applications) and cooking applications in rural areas from biomass energy. The graphical illustration of the combined biomass advanced micro-gasifier cookstove with ATEG system is shown in **Figure 2(a** and **b)**.

2.2 Characterisation of fuels

The two different categories of biomass used in the study are:

a. Solid biomass

(i) *Prosopis juliflora (Seemai Karuvelam)*

(ii) Coconut shells *(Thotti/Cherattai/Kottanguchi)*

b. Pellet (densified biowaste)

(iii) Tamarind seed pellet *(Puliyan kottai)*

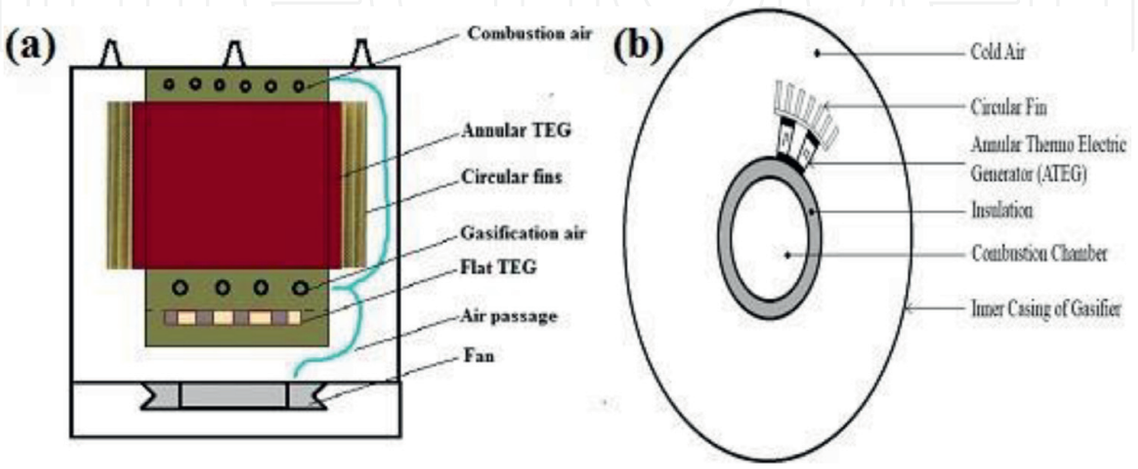

Figure 2.
(a) Advanced micro-gasifier annular thermoelectric generator system and (b) cross-sectional view.

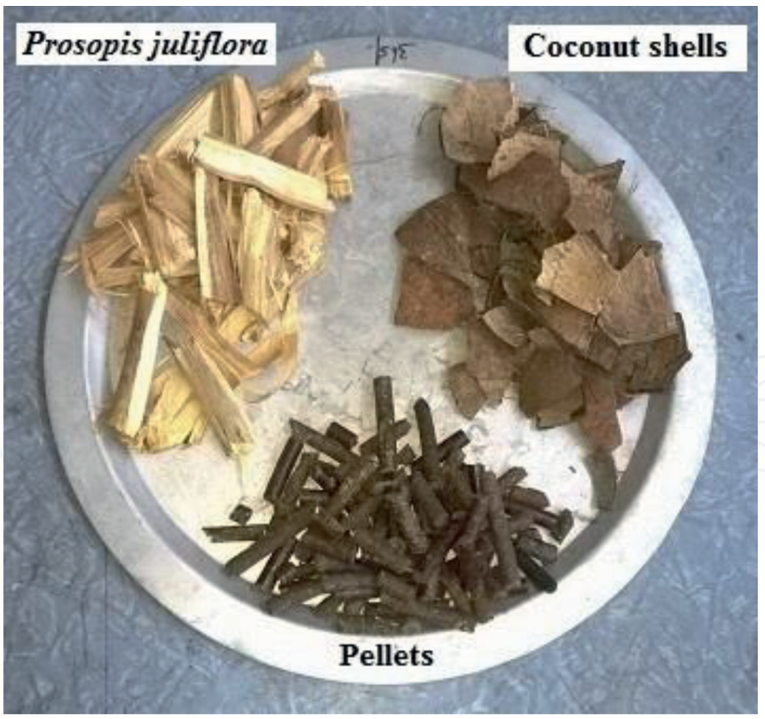

Figure 3.
Photograph of the biomass fuels considered for the experimental study.

Characteristics	*Prosopis juliflora*	Coconut shells	Tamarind seed pellet	Standard
Size (cm^3)	5 × 2 × 0.5	5 × 3 × 0.25	5 × 1	–
Bulk density (kg m^{-3})	560±20	610±20	1200±10	–
HHV (MJ/kg)	17.7	17.37	16.2	ASTM E711-87
Moisture content (%)	5.4	10	10.07	ASTM E871-82
Volatile matter (%)	77.9	72.05	63.02	ASTM E872-82
Ash content (%)	1.0	0.59	9.07	ASTM D1102-84
Fixed carbon (%)	15.7	17.34	18.04	*By difference*
Carbon (%)	45.5	45.84	50.15	ASTM E777-08
Hydrogen (%)	6.4	5.51	6.02	ASTM E777-08
Nitrogen (%)	0.6	0.35	0.42	ASTM E778-08
Oxygen (%)	47.2	47.58	41.41	*By difference*
Sulphur (%)	0.3	–	0.28	–

Table 1.
Proximate and ultimate analysis of the three different fuels [11–15]

The three types of biomass with different densities and ash content considered for this work are depicted in **Figure 3**, including two types of solid biomass wood with different properties and an agro residue seed pellet. All the solid biomass and pellets used are first dried in sunlight for 24 hours to ensure uniform moisture content (5–10%).

Table 1 summarises the properties of all the types of biomass used. Pictures of all the biomass types used in the experiments are illustrated in **Figure 3**.

3. Thermodynamic modelling

3.1 Thermodynamic modelling of the advanced micro-gasifier cookstove

The graphical illustration of the advanced micro-gasifier cookstove with the ATEG is presented in **Figure 4**. The thermal resistance network of the combined advanced cookstove ATEG is exposed in **Figure 5**.

By using the first law of thermodynamics, the energy balance equation of the biomass advanced cookstove ATEG can be written as

$$Q_{gen} = Q_{loss} + Q_{useful} \tag{1}$$

$$Q_{gen} = m_{fuel} \times CV_{fuel} \tag{2}$$

$$Q_{loss} = Q_{rad} + Q_{cond} + Q_{conv} \tag{3}$$

$$Q_{rad} = \sigma \varepsilon_{pan} A_{pan} \left({T_{pan}}^4 - {T_{air}}^4 \right) \tag{4}$$

$$Q_{cond} = Q = \frac{T_{cc} - T_h}{R_{s1} + R_{ins} + R_{s2} + R_{teg}} \tag{5}$$

$$Q_{conv} = \frac{T_h - T_c}{R_{air}} \tag{6}$$

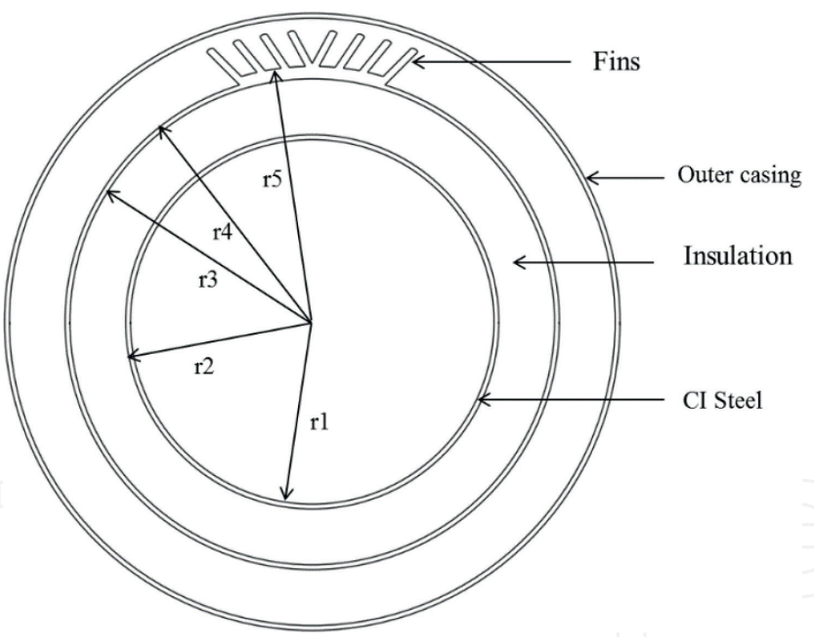

Figure 4.
Schematic illustration of the advanced micro-gasifier ATEG.

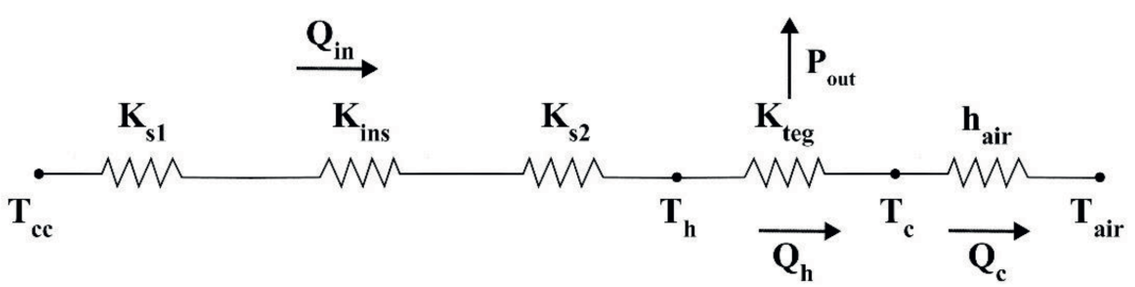

Figure 5.
The thermal network of advanced micro-gasifier ATEG.

3.1.1 Conductive resistance

Conductive resistance from a CC to ATEG (radial direction) is determined considering one-dimensional (1D) with steady-state conductive heat transfer via composite cylindrical walls. Three different types of materials, namely, steel-1 and steel-2 made up of extraordinary carbon steel, are used; the thermal insulation material used is Vermiculite composite:

$$R_{s1} = \frac{1}{2\pi k_{s1} L} ln \frac{r_2}{r_1} \tag{7}$$

$$R_{ins} = \frac{1}{2\pi k_{ins} L} ln \frac{r_3}{r_2} \tag{8}$$

$$R_{s2} = \frac{1}{2\pi k_{s2} L} ln \frac{r_4}{r_3} \tag{9}$$

$$R_{teg} = \frac{1}{2\pi k_{teg} L} ln \frac{r_5}{r_4} \tag{10}$$

3.1.2 Convective resistance

Convective resistance from ATEG to combustion air (radial direction) is considered as 1D steady-state convective heat transfer for ATEG (through extended surface finned annulus):

$$R_{air} = \frac{1}{2\pi h_{air} L r_5} \tag{11}$$

3.1.3 Heat transferred at hot and cold side junction of ATEG

Waste heat from the outer surface of CC is absorbed by the ATEG (Q_h) at the hot junction can be deliberated by the energy balance equation given as

$$Q_h = \alpha \mathrm{I} T_h - \frac{I^2 R}{2} + K(T_h - T_c) - \frac{\tau I (T_h - T_c)}{2} \times n \tag{12}$$

The transmitted heat through the ATEG is released at the cold side junction (annular fins) of the ATEG by preheating the combustion air. The equation is written as

$$Q_c = \alpha \mathrm{I} T_c + \frac{I^2 R}{2} + K(T_h - T_c) + \frac{\tau I (T_h - T_c)}{2} \times n \tag{13}$$

3.2 Thermodynamic modelling of ATEG

A cross-sectional observation of the thermoelement of an ATEG is depicted in **Figure 6**. The cross-sectional area A(r) of the ATEG thermoelectric pair increases in a radial direction (r). The exhaustive thermodynamic modelling and energy and exergy analysis of the ATEG in view of the Thomson effect have been deliberated in the following section, as studied by Kaushik and Manikandan [18]. The assumptions used for the thermodynamic modelling and investigations of ATEG are:

- 1D steady-state heat transfer equation of ATEG alongside the radial path is deliberated for the study.

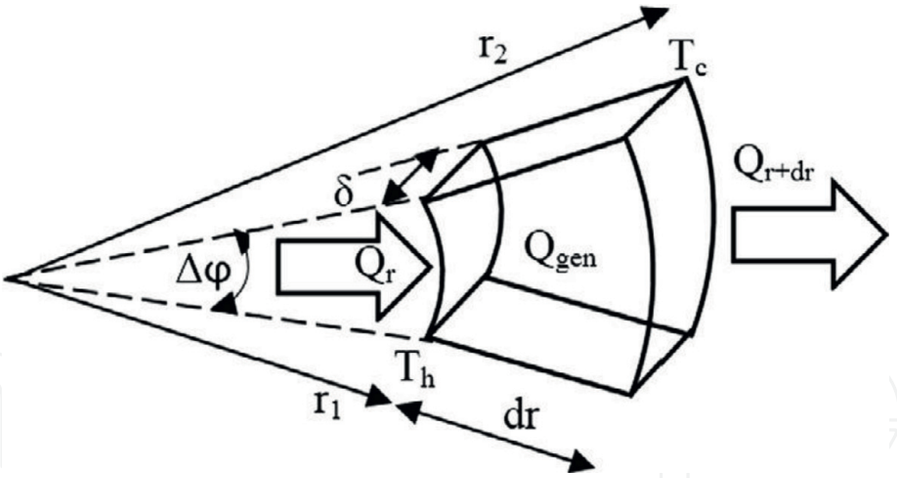

Figure 6.
Cross-sectional view of ATEG [1].

- The thickness (δ) of the ATEG module is constant throughout.
- Convection losses and radiation losses from the sides of the thermoelectric modules to the atmosphere are negligible (as heated air is recirculated into the combustion chamber).
- The electrical resistance of the contact is presumed to be about 10% of the actual inbuilt electrical resistance.

For the study, it has been assumed that $Q_{storage} = Q_{g,\,loss} = 0$; however Q_r and Q_{r+dr} are the heat input (from waste heat) supplied to the ATEG from outside the CC and heat output dissipated from the ATEG into the secondary air, respectively, whereas Q_{gen} can be the addition of Thomson and Joule's heat produced in the element (dr) [1]. The cross-sectional region of the thermoelement is established on the study conducted by Shen et al. [19].

Based on the assumptions, the cross-sectional area, length (L) and thickness (δ) of the p-type and also n-type thermoelectric (TE) leg are the same; the dispersal of temperature in the p-type and n-type leg of the ATEG is also assumed to be the same. Shen et al. [19] have studied the thermal conductance (K) and electrical resistance (R) of the ATEG are as given below:

$$K = \left(K_n + K_p\right) = \frac{\Delta\varphi\delta}{ln(r_5/r_4)}\left(k_n + k_p\right) \tag{14}$$

$$R = \left(R_n + R_p\right) = \frac{ln(r_5/r_4)}{\Delta\varphi\delta}\left(\rho_n + \rho_p\right) \tag{15}$$

The only difference is the value of K and R in the thermodynamic modelling of the FTEG and ATEG; the rest of the equations for the GATEG and GFTEG are comparable with Shen et al. (2015):

$$I = \frac{(\propto - \tau)(T_h - T_C)}{R + R_L} \tag{16}$$

$$R_L = \sqrt{1 + ZT_mR} \tag{17}$$

The thermal properties and electrical properties of a TE material combined together are referred to as figure of merit (FOM). Dimensionless FOM has been generally used to measure the desirability of TE materials for devices by multiplying with mean operating temperature (T_m) [1]:

$$ZT_m = \frac{\propto(\propto - \tau)}{\rho k}\frac{(T_h - T_C)}{2} \tag{18}$$

The power output (W) produced, electrical energy efficiency (%) and exergy efficiency (%) of an advanced micro-gasifier-based ATEG system can be considered from the altered work done by Manikandan and Kaushik [1]:

$$P_{out} = Q_h - Q_c = (\alpha - \tau)(T_h - T_c)I - I^2R = I^2R_L \tag{19}$$

Eq. (19) designates that the Thomson effect will decrease the power output of the ATEG. The energy efficiency (electrical) of advanced cookstove-assisted ATEG is given as

$$\eta_{el} = \frac{P_{out}}{Q} = \frac{(\alpha - \tau)(T_h - T_c)I - I^2R}{Q_{cond}} \times n \tag{20}$$

The exergy efficiency (electrical) of the advanced cookstove-assisted ATEG is derived as

$$\psi_{el} = \frac{P_{out}}{E_Q} = \frac{(\alpha - \tau)(T_h - T_c)I - I^2R}{Q_{cond}\left(1 - \frac{T_{air}}{T_h}\right)} \times n \tag{21}$$

Hence, the combination of potential energy and exergy efficiencies of the advanced micro-gasifier cookstove ATEG system can be written as

$$\text{Combined efficiency } (\%) = \eta_{el} + \eta_{th} \tag{22}$$

The energy as well as exergy analysis of the micro-GATEG is analysed via engineering equation solver (EES) for different operating conditions.

3.3 Cookstove performance

3.3.1 Energy efficiency

Thermal efficiency (%) is defined as the fraction of heat energy given off by the biomass fuel that is successfully transported to the water in the cooking vessel. The remaining unrecovered heat energy is dissipated into the largest heat sink of an atmosphere. The method used to assess the thermal energy efficiency is specified in Eq. 23, as follows:

$$\eta th = \left\{\frac{\left[4.186 \times \left(m_{wi} - m_{wf}\right) \times \left(T_{wf} - T_{wi}\right)\right] + (W_v \times 2257)}{m_{fw} \times CV_{fuel}}\right\} \tag{23}$$

3.3.2 Exergy efficiency

The maximum possible work, which can be created by a system for a particular environmental condition, is generally taken as the Carnot hypothetical maximum

relating to the ambient temperature. The thermal exergy input supplied to the pot for water boiling can be stated as below [13, 14, 20]:

$$\text{Exin} = (m\text{TP} \times C1 \times \eta c + \text{x} \times d \times \text{C2})\left(1 - \frac{Ta}{T\text{fuel}}\right) \tag{24}$$

The exergy output of the ATEG attached advanced micro-gasifier cookstove is the quantity of energy spent by the boiling water times the Carnot factor as follows [20]:

$$\text{Ex}o = \left\{mw \times Cp \times (T\text{fw} - \text{Tiw})\left(1 - \frac{Ta}{T\text{fw}}\right) + \text{mpot} \times \text{Cp, pot} \times (T\text{fp} - \text{Tip})\left(1 - \frac{Ta}{T\text{fp}}\right)\right\} \tag{25}$$

Generally, lowering heat source or raising heat sink lowers exergy. The exergy efficiency (ψ) is well defined as the fraction between the output exergy and the input exergy as shown below:

$$\eta\text{th} = \frac{\text{Ex}o}{\text{Exin}} \tag{26}$$

A small number of essential parameters like the mass of water (kg), the weight of fuel (kg), the volume of the kerosene sample (for the ignition of fuel) and the weight of unfilled Al vessel were computed before starting the test. Readings of water temperature (°C) and pot temperature (°C) were taken on a minute-to-minute basis. The reference conditions taken for exergy analysis are To=303 K and Po=101.325 kPa.

4. Results and discussions

4.1 Analysis of energy and exergy efficiencies of the advanced micro-gasifier cookstove

The performance of the ACS cookstove is assessed in terms of energy efficiency (%) and exergy efficiency (%) using *Prosopis juliflora*, coconut shells and tamarind seed pellets as fuel. It is perceived that the thermal efficiencies of the stove are 36.7±0.4, 37±0.4 and 35±0.4% for coconut shell, *Prosopis juliflora* and tamarind pellets, respectively, after four repetition tests. The exergy efficiencies (%) of the cookstove are 15.6±0.45, 17.5±0.45 and 15±0.45% for the discussed three different fuels. The uncertainties for energy and exergy efficiencies are established as 0.43% and 0.48%, respectively.

The comparison on the energy efficiency and exergy efficiency of the advanced micro-gasifier cookstove is illustrated in **Figure 7** for a distinct set of operational constraints. It is also witnessed that the energy efficiency (%) performance of the ACS cookstove is considerably higher than that of exergy efficiency (%) performance. This is due to the extent of energy extracted in the hot water for ACS cookstove being much less than the worth of energy extracted due to temperature constraint; this phenomenon is common for all cookstoves.

4.2 Conceptual modelling results of GATEG

In this investigative study, the energy and exergy analysis of an advanced micro-gasifier cookstove ATEG is studied under various operating circumstances. The

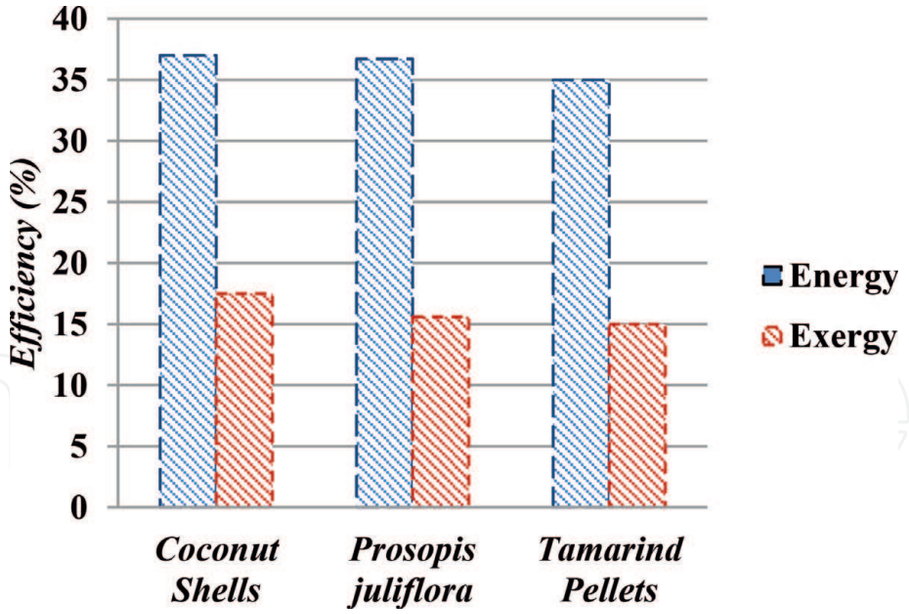

Figure 7.
Energy and exergy efficiencies of the advanced micro-gasifier cookstove.

influence of hot side and cold side junction temperature and the influence of the number of thermocouples and operating electric current (A) on electric power output (W), thermal output (of cookstove) and energy and exergy efficiencies (%) of the GATEG system are studied.

4.2.1 Effect of change in hot junction temperature

The influence of CC temperature outside the insulation on the power output as well as the energy and exergy efficiencies (%) of the ATEG have been studied. The combustion air temperature passed over the annular fins of the TEG varies with time so the cold junction temperature is also varied between 30 and 150°C in this study. The atmospheric temperature is considered as 30°C.

The effects of various hot junction temperatures on the power output of the ATEG are shown in **Figure 8(a–f)**. The various zones of the CC temperature determine the hot side temperature of the ATEG. During combustion of the advanced micro-gasifier cookstove, the flame front propagates downwards with respect to the fuel bed density and heat transfer rate. Hence, heat is not uniform throughout from top to bottom. The uniform temperature is reached only after the conversion takes place from volatile combustion mode to char combustion mode, almost at the end (after 70% of weight loss in fuel). Therefore, when there is a variation in hot junction temperature, like an increase from a smaller value to higher, the power output (W) and the optimum current (A) value for maximum power output also increase. The reason is that when the temperature inside the combustion zone increases, a respective temperature of the outside chamber after insulation increases, thus increasing the power output of the TEG. It is also clear from **Figure 8(a–f)** that the power output of the micro-gasifier annular thermoelectric generator is maximum when the outside combustion temperature is at a maximum of 275°C. At a current flow rate of 0.8 A, the actual power output of GATEG is 10.05 W, electrical energy efficiency is 6.76% and exergy efficiency is 15%.

Similarly, from **Figure 8(a–f)**, it is clear that the power output of the micro-gasifier ATEG is minimum when the outside combustion temperature is at a minimum of 150°C. At a current flow rate of 0.4 A, the power output of GATEG is 2.414 W, electrical energy efficiency is 1.31% and exergy efficiency is 4.62%.

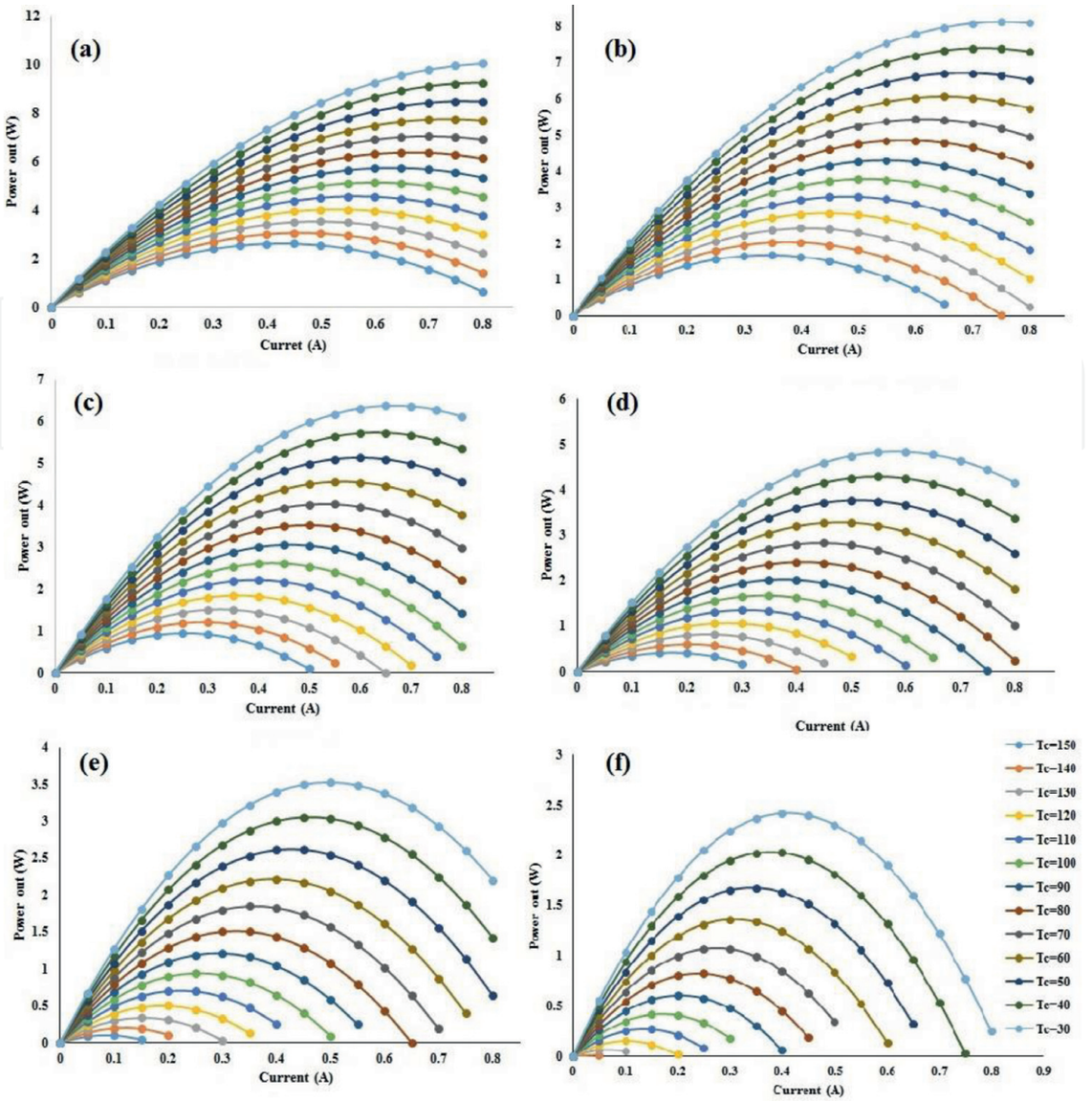

Figure 8.
Power output (W) with respect to current (A) for (a) 275°C, (b) 250°C, (c) 225°C, (d) 200°C, (e) 175°C and (f) 150°C.

The influence of variation of hot lateral temperature on the electrical energy efficiency (%) of GATEG is shown in **Figure 9(a–f)**. It can be observed from **Figure 9(a–f)** that the electrical energy efficiency of GATEG is for the range of heat input considered, for the maximum hot side temperature of 275°C and an operational current flow of 0.8 A; the electrical efficiency (%) of GATEG is 6.76%.

The variation of exergy efficiency of GATEG for changing cold junction temperatures at maximum hot side temperature of 275°C is shown in **Figure 10(a–f)**. It is seen that the exergy efficiency of the GATEG is high for all working conditions. It is obvious that the exergy efficiency of GATEG obtained for the heat input of 149 W at a working current of 0.8 A is 6.76%. This is due to the power output (i.e., exergy output) of the GATEG that is marginally greater because of superior heat transfer rates.

4.2.2 Effect of the number of thermocouples

The influence of the number of thermo-plates (i.e., thermocouples) on the performance variance like power output (W), energy efficiency and exergy

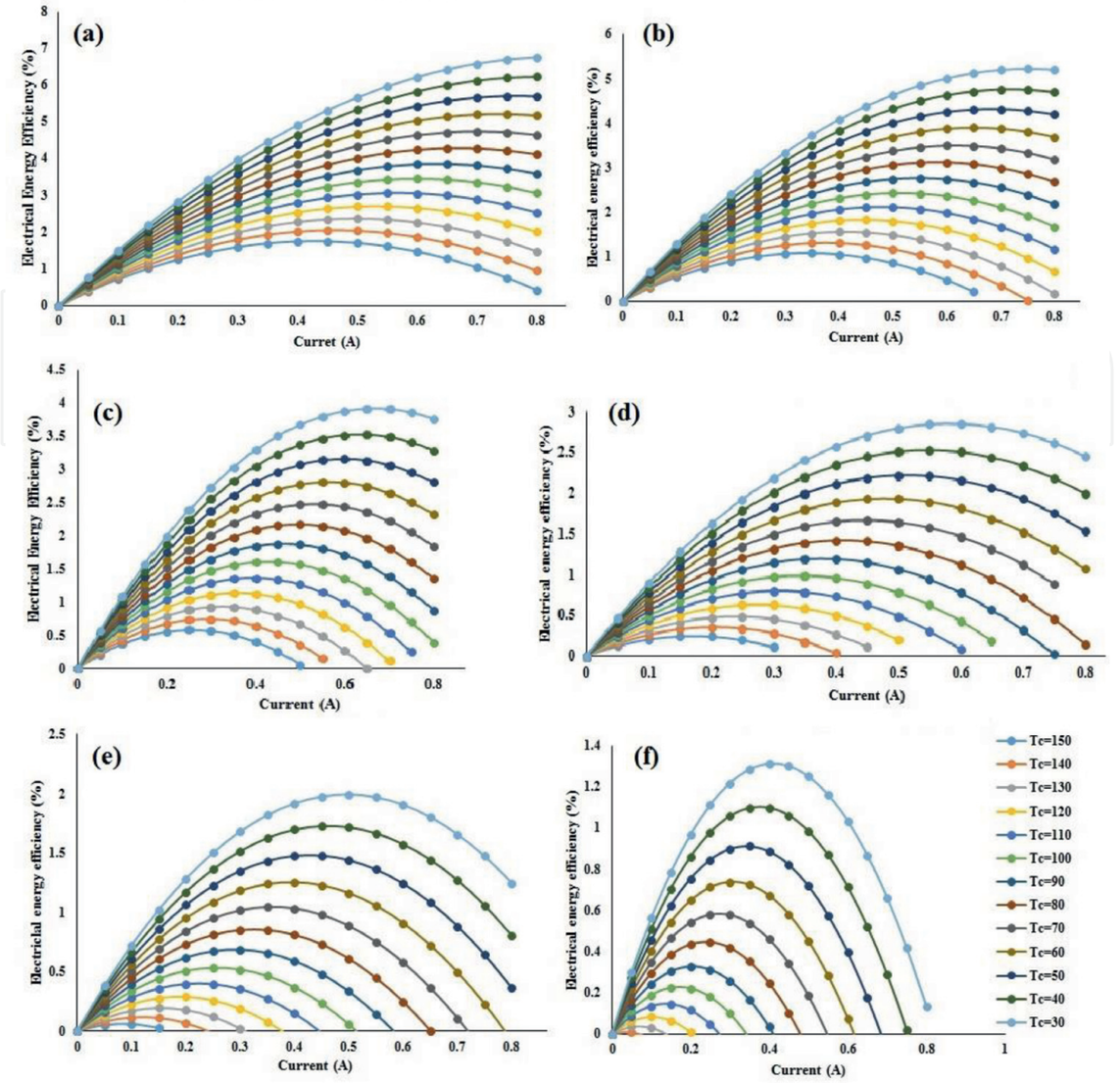

Figure 9.
Electrical energy efficiency (%) with respect to current (A) for (a) 275°C, (b) 250°C, (c) 225°C, (d) 200°C, (e) 175°C and (f) 150°C.

efficiency of the ACS cookstove annular/flat thermoelectric generator cogeneration system is studied. With an increase in the number of thermocouples, there is a rise in the heat transfer area. Hence, heat transfer between a hot side and cold side junction of the ATEG system is improved, as deliberated by Manikandan and Kaushik [1] and He et al. [21]. **Figure 11** shows the effect of numbers in thermocouples on the power output (W) of GATEG, with a clear indication of the number of thermocouples being directly proportional to the power output of GATEG, as proposed by Manikandan and Kaushik [1].

The hot junction temperature is considered as 275°C, and the cold side temperature is retained at 30°C. The losses in the systems are considered as negligible. **Figure 11** demonstrates the influence of the number of TEG modules on the electric power generation for variation of current (A) levels. **Figure 11** clearly indicates the power produced; it is maximum as a result of the addition of/rises in the number of TEG modules.

Eventually, the addition of modules leads to overall thermal resistance causing a reduction in the combined modules, R_{tem}, which leads to a fall in temperature difference, rapidly offsetting any further rise in voltage output. The plots shift to small current range slowly as "n" increases primly due to the interior electrical resistance upsurges steadily with the number of modules. The maximum power

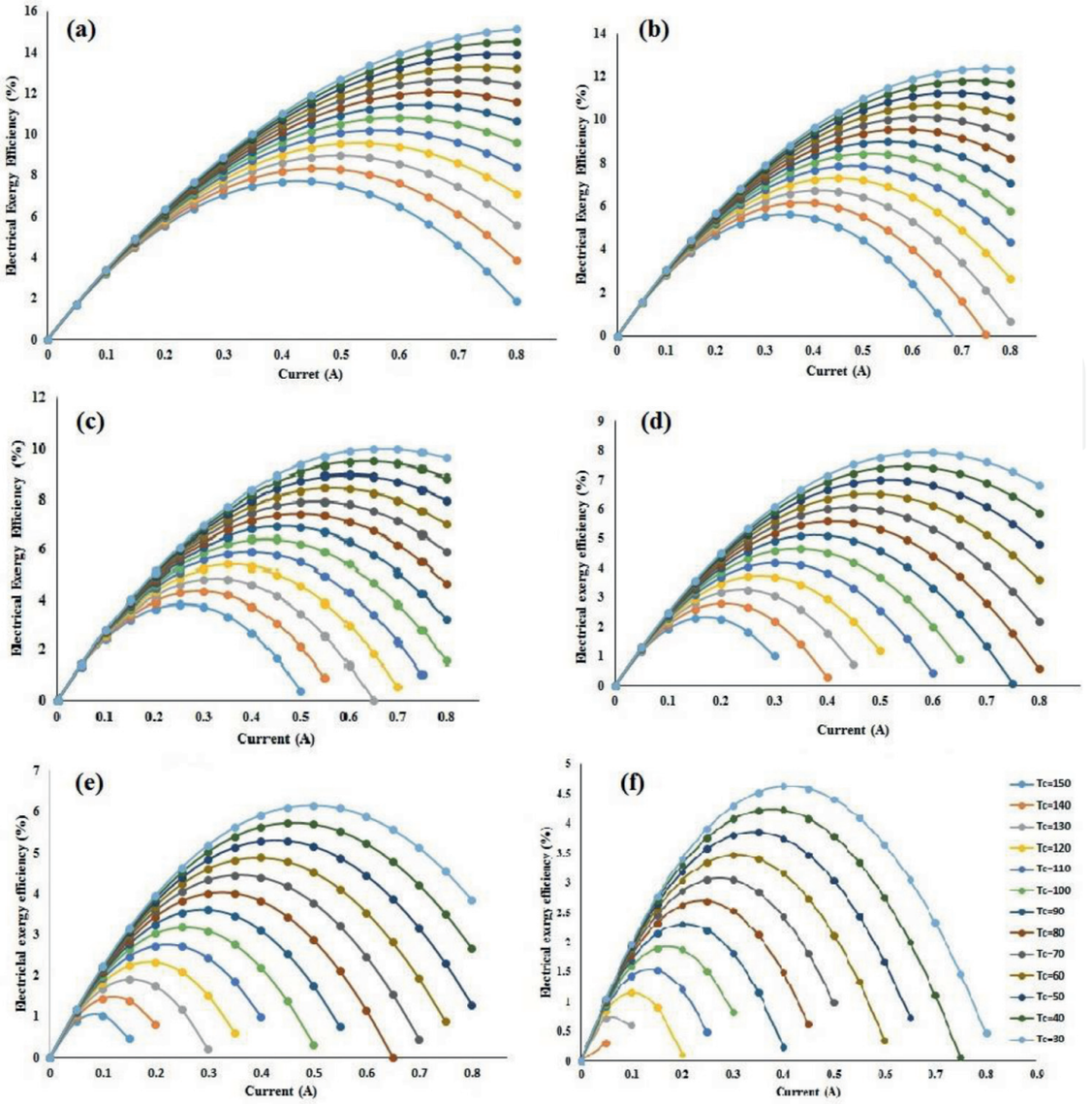

Figure 10.
Electrical exergy efficiency (%) with respect to current (A) for (a) 275°C, (b) 250°C, (c) 225°C, (d) 200°C, (e) 175°C and (f) 150°C.

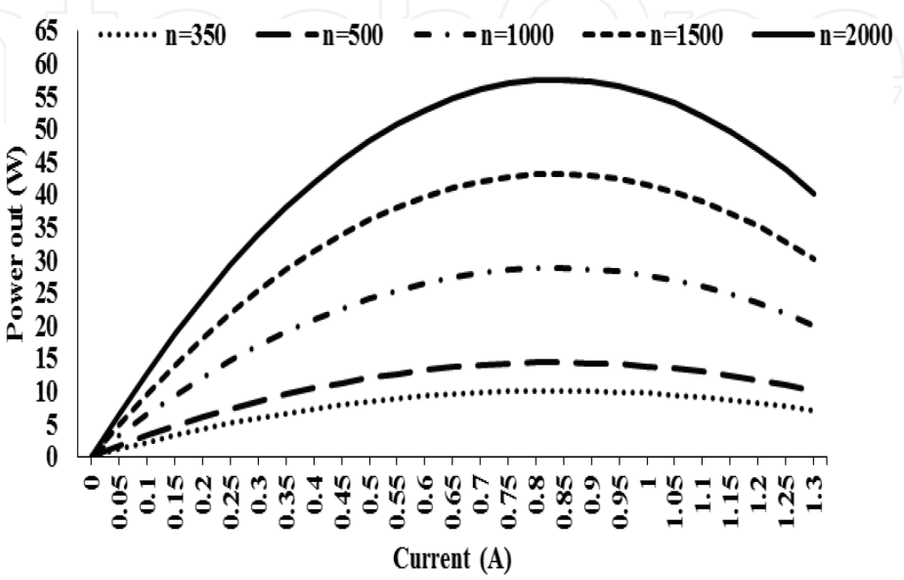

Figure 11.
Influence of the number of TEG modules on the power output.

(W) is obtained once the load resistance (R_L) matches with the system resistance according to maximum power transfer theorem. A similar curve with a notable difference in power output indicates that the maximum power output is attained for an increasing number of thermoelectric modules. The increase in efficiency by increasing 100 numbers into 1000 numbers is 100%. Thus, from the power output point of view, using an increased number of modules produces more power. This observation is similar to that of a steady state conducted by Jie Chen et al. [22]. A further intensification in the number of thermocouples results in an increase in surface area and volume which offers more resistance, thereby increasing the temperature of combustion air and consequently reducing the power output of TEG (refer **Figure 11**) and its electrical energy efficiency. These outcomes are comparable to those recorded by He et al. [21, 23].

5. Conclusions

An investigation of the micro-gasifier ATEG is conducted based on the first law and second law of thermodynamics, and its performance factors are investigated for varying hot and cold side temperature conditions and by varying number of thermocouples. From the conceptual modelling, the following conclusions are summarised:

- The power output (W), electrical energy efficiency (%), exergy efficiency (%) and combined system energy and exergy efficiencies (%) of the GATEG are 10.05 W, 6.76%, 15.12% and 43.46% and 30.72%, respectively, calculated for the maximum temperature difference of 275°C across the TEG, with the help of EES software.

- The same modelling is repeated for a low surface temperature of 150°C outside the combustion chamber. The power output (W), electrical energy efficiency (%), exergy efficiency (%) and combined system energy efficiency (%) of the GATEG are 2.41 W, 1.31%, 4.63% and 38% and 20.23%, respectively, for the maximum temperature difference of 150°C across the TEG.

- The advanced micro-gasifier cookstove annular thermoelectric generator is a suitable option since it has many advantages like enhanced heat transfer characteristics in the hot side and cold side of the ATEG due to the greater heat transfer area. The diameter (D) of the CC (based on the cooking load requirement) can be increased if necessary, to provide more heat transfer surface area to the ATEG.

The fixing of the ATEG with the cylinder-shaped CC will be very easy, and the facility to arrange for thermal insulation to the cold lateral of the TEG will become easier if the ATEG has been adopted. The conceptual model analysis untaken in this study may be supportive in designing actual GATEG systems for electric power production from engine exhaust heat (flue gas), other heat pipes, etc. As the power output (W) and overall exergy efficiency (%) of the GATEG are low, these arrangements are improvident, but with the improved/novel TEG materials with the higher ZT, this type of concepts will gain more significance in the near future.

Nomenclature

Q_{gen}	heat generated inside the combustion chamber of gasifier (W)
Q_{loss}	heat loss by conduction, convection and radiation (W)
Q_{useful}	the heat input to the purpose of water boiling (W)
m_{fuel}	mass rate of fuel consumed (kg/s)
CV_{fuel}	calorific value of wood (kJ/kg)
Q_{rad}	radiation loss offered by the pan (W)
σ	Stefan-Boltzmann constant (W/m^2K^4)
ε_{pan}	emissivity of the pan
A_{pan}	surface area of the pan (m^2)
T_{pan}	final temperature of the pan (K)
T_{air}	atmospheric air temperature (K)
$Q_{cond} = Q$	heat input to the ATEG (W)
T_{cc}	temperature inside the combustion chamber (K)
T_h	temperature at hot junction of ATEG (K)
R_{s1}	conductive resistance for steel-1 (K/W)
R_{ins}	conductive resistance for insulation (K/W)
R_{s2}	conductive resistance for steel-2 (K/W)
R_{teg}	conductive resistance for ATEG (K/W)
Q_{conv}	heat rejected by the cold junction of ATEG (W)
T_h	temperature at hot junction of ATEG (K)
T_c	temperature at cold junction of ATEG (K)
k_{s1}, k_{s2}	thermal conductivities of steel-1 and steel-2 (W/m K)
k_{ins}	thermal conductivity of insulation (W/m K)
K_{teg}	thermal conductivity of TEG (W/m K)
L	length of the combustion chamber or ATEG (m)
r_1	inner diameter of combustion chamber or steel-1 (m)
r_2	outer diameter of steel-1 and inner diameter of insulation (m)
r_3	outer diameter of insulation and inner diameter of steel-2 (m)
r_4	outer diameter of steel-2 and inner diameter of ATEG (m)
r_5	outer diameter of ATEG (m)
h_{air}	convective heat transfer coefficient (W/m^2K
Q_h	heat absorbed by the hot junction of the ATEG (W)
Q_c	heat rejected by the cold junction of the ATEG (W)
K	thermal conductance of the ATEG (W/K)
R	electrical conductance of the ATEG (Ω)
φ	angle (radians)
k_p, k_n	thermal conductivity of p and n legs of ATEG (W/m K)
ρ_n, ρ_p	electrical resistivity of p and n legs of ATEG (Ωm)
I	current (A)
α	Seebeck coefficient (V/K)
τ	Thompson coefficient (V/K)
R_L	external resistive load of imposed on ATEG (Ω)
ZT_m	dimensionless figure of merit
Z	figure of merit (1/K)
P_{out}	power output from the ATEG (W)
n	no of thermoelectric couples
η_{el}	electrical energy efficiency (%)
ψ_{el}	exergy efficiency (%)

Author details

Sakthivadivel Duraisamy[1*], Manikandan Sundararaj[3], Kumaraselvan Raja[2], Ganesh Kumar Poongavanam[2] and Iniyan Selvarasan[2]

1 School of Mechanical Engineering (SMEC), Vellore Institute of Technology (VIT) University, Vellore, Tamil Nadu, India

2 Department of Mechanical Engineering, Institute for Energy Studies, College of Engineering Guindy Campus, Anna University, Chennai, India

3 SRM Institute of Science and Technology, Tamil Nadu, India

*Address all correspondence to: sakthi2energy@gmail.com

References

[1] Manikandan S, Kaushik SC. Energy and exergy analysis of solar heat pipe based annular thermoelectric generator system. Solar Energy. 2016;**135**:569-577

[2] Karri MA, Thacher EF, Helenbrook BT. Exhaust energy conversion by thermoelectric generator: Two case studies. Energy Conversion and Management. 2011;**52**:1596-1611

[3] Champier D, Bedecarrats JP, Rivaletto M, Strub F. Thermoelectric power generation from biomass cookstoves. Energy. 2010;**35**:935-942

[4] Nuwayhid RY, Shihadeh A, Ghaddar N. Development and testing of a domestic woodstove thermoelectric generator with natural convection cooling. Energy Conversion and Management. 2005;**46**:1631-1643

[5] Kraemer D, Poudel B, Feng HP, Caylor JC, Yu B, Yan X, et al. High-performance flat-panel solar thermoelectric generators with high thermal concentration. Nature Materials. 2011;**10**:532-538

[6] Omer SA, Infield DG. Design optimization of thermoelectric devices for solar power generation. Solar Energy Materials & Solar Cells. 1998;**53**:67-82

[7] Omer SA, Infield DG. Design and thermal analysis of a two stage solar concentrator for combined heat and thermoelectric power generation. Energy Conversion and Management. 2000;**41**:737-756

[8] Atik K. Numerical simulation of a solar thermoelectric generator. Energy Source Part A. 2011;**33**:760-767

[9] Chen G. Theoretical efficiency of solar thermoelectric energy generators. Journal of Applied Physics. 2011;**109**: 104908-1041–8

[10] Raman P, Murali J, Sakthivadivel D, Vigneswaran VS. Performance evaluation of three types of forced draft cookstoves using fuel wood and coconut shell. Biomass and Bioenergy. 2013;**49**: 333-340

[11] Sakthivadivel D, Balakumar A, Iniyan S. Development of advanced cookstove with optimum air mixture using CFD. Asian Journal of Research in Social Sciences and Humanities. 2017; **7**(2):384-392

[12] Sakthivadivel D, Iniyan S. Combustion characteristics of biomass fuels in a fixed bed micro-gasifier cookstove. Journal of Mechanical Science and Technology. 2017;**31**(2): 995-1002

[13] Sakthivadivel D, Iniyan S. Characterization, density and size effects of fuels in an advanced micro-gasifier stove. Biofuels. 2018;**31**(2): 995-1002

[14] Sakthivadivel D, Iniyan S. Experimental design and 4E (energy, exergy, emission and economical) analysis of a fixed bed advanced micro-gasifier stove. Environmental Progress & Sustainable Energy. 2018;**37**(6): 2139-2147

[15] Sakthivadivel D, Ganesh Kumar P, Iniyan S. Computational modeling and performance evaluation of an advanced micro-gasifier cookstove with optimum air injection. Biofuels. 2019. https://doi.org/10.1080/17597269.2019.1573606

[16] Tryner J, Tillotson JW, Baumgardner ME, Mohr JT, MW DF, Marchese AJ. The effects of air flow rates, secondary air inlet geometry, fuel type, and operating mode on the performance of gasifier cookstoves. Environmental Science & Technology. 2016;**50**:9754-9763

[17] BIS. Method of test for thermal conductivity of thermal insulation materials by means of heat flow meter (First Revision of IS 9489). In: Bureau of Indian Standards. 2015

[18] Manikandan S, Kaushik SC. Energy and exergy analysis of an annular thermoelectric cooler. Energy Conversion and Management. 2015;**106**: 804-814

[19] Shen ZG, Wu SY, Xiao L. Theoretical analysis on the performance of annular thermoelectric couple. Energy Conversion and Management. 2015;**89**:244-250

[20] Tyagi SK, Pandey AK, Sahu S, Bajala V, Rajput JPS. Experimental study and performance evaluation of various cookstove models based on energy and exergy analysis. Journal of Thermal Analysis and Calorimetry. 2013;**111**: 1791-1799

[21] He W, Su Y, Wang Y, Riffat S, Ji J. A study on incorporation of thermoelectric modules with evacuated-tube heat-pipe solar collectors. Renewable Energy. 2012;**37**(1):142-149

[22] Chen J, Zuo L, Wu Y, Klein J. Modeling, experiments and optimization of an on-pipe thermoelectric generator. Energy Conversion and Management. 2016;**122**: 298-309

[23] He W, Su Y, Riffat S, Hou J, Ji J. Parametrical analysis of the design and performance of a solar heat pipe thermoelectric generator unit. Applied Energy. 2011;**88**(12):5083-5089